Title
FEASIBILITY TESTS OF A HIGH RESOLUTION SAMPLING RADIAL DRIFT CHAMBER

Authors
Huth, J.
Nygren, D.

Publication Date
1985-05-01

LBL-19462

Lawrence Berkeley Laboratory
UNIVERSITY OF CALIFORNIA

Physics Division

Submitted to Nuclear Instruments and Methods

FEASIBILITY TESTS OF A HIGH RESOLUTION SAMPLING RADIAL DRIFT CHAMBER

J. Huth and D. Nygren

May 1985

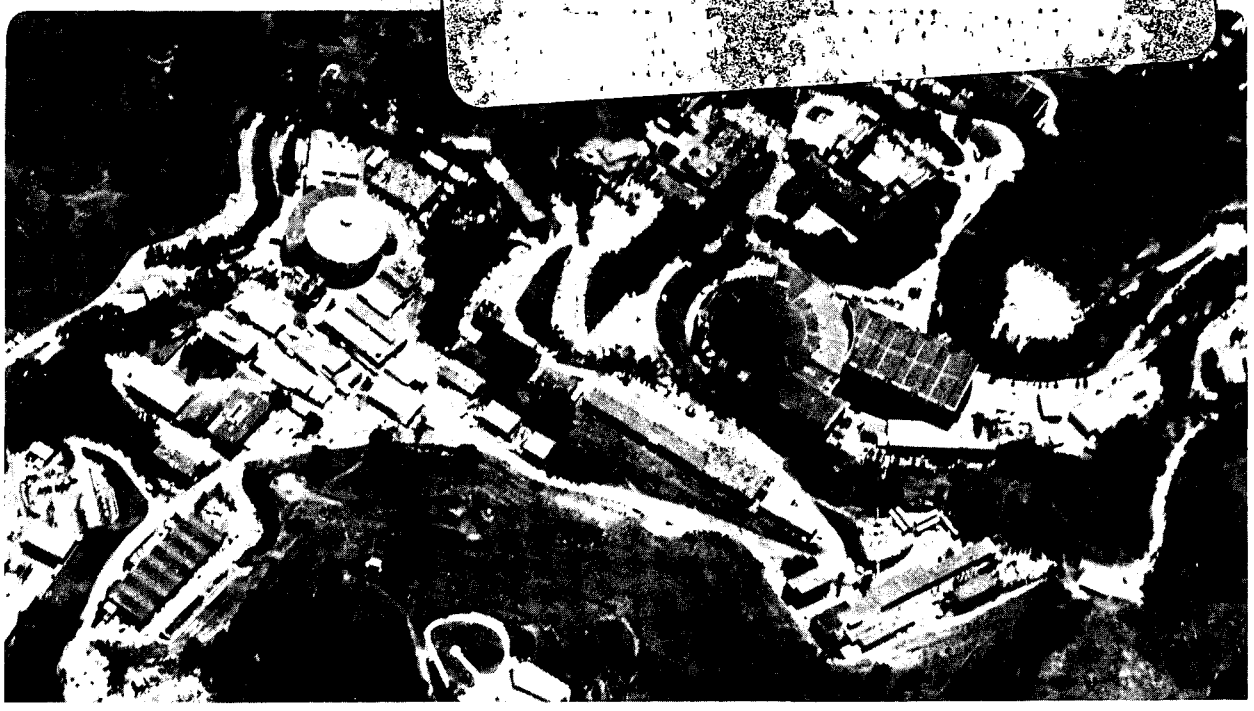

Prepared for the U.S. Department of Energy under Contract DE-AC03-76SF00098

LBL-19462

DISCLAIMER

Feasibility Tests of a High Resolution Sampling Radial Drift Chamber

John Huth *

Department of Physics and Astronomy, University of Massachusetts, Amherst, MA 01003, USA

David Nygren

Lawrence Berkeley Laboratory, University of California, Berkeley, CA 94720, USA

TPC-LBL-85-7

LBL-19462

14 May, 1985

Abstract

The design concept and results of feasibility tests for a vertex detector intended for use in the TPC-PEP4/9 experiment are presented. The detector is based on a slow radial drift in dimethyl ether. High resolution localization of the avalanches at the sense wire is accomplished with nearby pickup wires and the utilization of waveform sampling electronics. The avalanche angular coordinate measurements, combined with knowledge of the electric field distribution and drift velocity permit reconstruction of the trajectory using essentially all track information. Measurements with a test chamber constructed to study characteristics of avalanche localization indicate that the recoverable track information in one centimeter of dimethyl ether at 1.5 atm is equivalent to 30 measurements of 40 μm accuracy.

*Present address: Fermi National Accelerator Laboratory, Batavia, IL 60510, USA.

Recent innovations in wire chamber technology [1]-[4] have led to the design of a novel vertex detector for use in the PEP-4 TPC/PEP-9 experiment at the Stanford linear accelerator center. This detector features a radial drift of ionization electrons in a slow, cool organic gas, dimethyl ether (DME, drift velocity $\approx 1\ cm/\mu sec$), combined with the use of pickup wires and waveform sampling to reconstruct track coordinates through avalanche localization. In this paper, we describe a preliminary design of the radial drift chamber (RDC), a discussion of the factors affecting spatial resolution, and the results from a test chamber used to measure some of these factors, in particular the use of pickup wires to reconstruct avalanche coordinates.

1 The radial drift chamber

Some recent trends in the development of drift chamber techniques are the use of induced signals on cathodes [1] and the related use of pickup wires to localize avalanche coordinates [2], the use of waveform sampling with subsequent pulse reconstruction [3], and the use of slow organic gases with limited diffusion [4]. These ideas have been incorporated into the design of the radial drift chamber (figure 1) [5]. The radial drift chamber consists of three cylindrical shells and two cylindrical, axial wire arrays. The innermost shell is the beam pipe, followed by (moving out in radius) an instrumented layer of wires, a central cathode, an outer layer of wires and an outer pressure wall. With the central cathode held at negative high voltage, ionization formed in the inner half of the chamber will drift to the inner set of wires, and the ionization formed outside the cathode will drift to the outer set of wires.

The reconstruction of tracks with the RDC is based on the concept that every point in the sensitive volume is mapped by the electric field to a corresponding position on the surface of an anode wire. This position on the anode wire can be defined by an angular coordinate α (figure 2). An electron cluster from a charged particle will arrive from its point of origin within the sensitive volume at the anode surface at a particular time t and angle α. Therefore, knowledge of the electric field configuration and drift velocity, combined with a measurement of $\alpha(t)$ will permit the reconstruction of the cluster origin. A typical track in the RDC will consist of a string of ionization clusters arriving sequentially up to the maximum drift time, producing a corresponding string of $\alpha(t)$ values. Because the typical track is nearly parallel to the electric field, the rate of change of α is small, and little, if any, information is lost if the signal processing electronics integrates over several clusters. The sensitivity to errors in drift velocity is greatly diminished relative to traditional techniques.

The resolution in α achievable in practice is crucial to the RDC. Factors contributing to the resolution include transverse diffusion during drift to the anode array, heating of the electrons in the transition region near an anode wire, and the avalanche process itself. The first two contributions can be estimated from currently available literature but there are relatively few studies of the properties of avalanche development [6] - [8], and none have been reported as yet for avalanches in DME.

In pure DME, transverse diffusion is expected to be much smaller than in traditional gas mixtures (figure 4). DME also displays an exceptional capacity to moderate electron temperature, even at high electric fields [9]. The absence of argon, traditionally a major component in drift chamber gas mixtures, eliminates a strong source of UV photons which can broaden the avalanche growth. Furthermore, in an avalanche dominated by collision processes, only the first few generations contribute significantly to fluctuations in the transverse growth of the avalanche. These considerations taken together suggested that the situation for measurement of $\alpha(t)$ in DME might be favorable, and may even offer a means to achieve superior resolution.

To measure α, we adopt the technique of using a pair of pickup wires placed near the anode, as suggested by Walenta [10] in his modified concept of the time expansion chamber (TEC). The asymmetry in the induced signals observed on the pickup wires is used to determine α, and hence track coordinates. The sense wire and its associated pickup wires

are hereinafter referred to as 'triplets'. In addition, field shaping wires are placed at the cell boundaries to optimize the electrostatic configuration (α_{max}), the electrostatic stability, amplification, and cell-to-cell signal isolation.

In the TEC concept, the wire plane configuation is arranged so that the particle trajectories of interest have small θ angles. The quantity of central interest is the distance perpendicular to the wire plane of the collected track segment. The existence of the pickup wires allows a correction to be made for the impact of ionization fluctuations along the collected track segment if the associated sampling circuitry is sufficiently fast to follow the azimuthal time development of the avalanches. However, as the track angle θ becomes smaller, the ionization clusters begin to merge in arrival time, complicating or preventing useful corrections.

In contrast, the particle trajectories of interest for the RDC are approximately radial ($\theta \approx 90^{o}$), parallel to the drift direction. This configuration allows all track information to be collected with negligible systematic error in $\alpha(t)$ over a wide range of θ. The time interval between cluster arrival is maximized, and the rate of change of the azimuthal coordinate α is typically small. Another aspect in which the radial drift chamber differs fundamentally from the TEC is the absence of a grid structure to separate the drift and amplification regions. The radial drift chamber also differs fundamentally from the TEC in the absence of a grid structure to separate the drift and amplification regions. In addition to offering a mechanical simplification, the absence of a grid in the RDC removes a source of track distortion and dispersion.

It is worth noting that the RDC represents a natural solution to the physical boundary constraints of colliding beam experiments; *viz* the existence of a grounded cylindrical beam pipe and, at a somewhat larger radius, a grounded cylindical enclosure of a large tracking device. In addition, the RDC is continuous in azimuth, requiring no field shaping structures other than the three concentric cylindrical shells.

Perhaps the most significant feature of the RDC is the unprecedented capability to exploit efficiently all track ionization (except δ rays) for the determination of the particle trajectory. In comparison, conventional 'transverse' drift chambers detect only the first electron of a track segment to arrive at a sense wire. The remainder of the track segment is ignored, although at the moment of creation, each ionization electron within the track segment contains statistically equivalent information. In contrast, the RDC can utilize essentially all of the track information. This feature permits, with the temporary assumption that all other sources of systematic error can be ignored, measurement precision which can be characterized by:

$$\sigma_x = \sqrt{\frac{\sigma_D^2 + \sigma_A^2}{n_e} + \sigma_e^2} \tag{1}$$

where

σ_x = measurement accuracy of a track segment of n_e electrons

σ_D = electron transverse diffusion averaged over the track segment drift distance

σ_A = contribution of avalanche processes expressed in equivalent spatial resolution

σ_e = electronic noise expressed in equivalent spatial resolution

In dimethyl ether, a yield of $n_e = 120/cm - atm$ is expected for total ionization. If the avalanche noise and electronic noise are assumed negligible, the data of figure 4 imply the possibility that one could obtain in one centimeter of track in dimethyl ether at 1 atm a measurement precision of less than $5\mu m$. This example illustrates the high intrinsic information content of tracks under ordinary conditions, as well as the gap in reported performance of traditional techniques which lie in the range of 20 to 80 μm [11]. Of the three terms in equation 1, the least well-known and conceivably dominant term is σ_A. In this work, we report results for σ_A in DME, which is an appropriate gas for the RDC.

In addition to the above advantages for charged particle tracking, the geometry has other desirable characteristics. When a track formed at the event vertex passes through both layers of instrumented wires, prompt ionization signals can be collected from the track segments closest to the wires within 50 *nsec*. This prompt information can be used for a momentum dependent trigger by requiring coincidences between prompt signals found on the inner and outer layers.

Because the drift velocity is slow in DME, the Lorentz angle is also small ($\approx 1^o$ in a 1.5 T field) making track reconstruction simpler. The geometry of the chamber also allows for a simple calibration of the Lorentz angle based on a relatively small amount of data. Segments of the same track in the inner and outer halves of the chamber will exhibit a kink if reconstructed assuming perfectly radial drift paths. By knowing the length of this kink and the total drift length, it is straightforward to calculate the Lorentz angle to the needed precision.

In the expected mode of operation, the chamber will operate at a pressure of 1.5 to 2.0 *atm* in dimethyl ether. Under these conditions we expect a yield of 180 to 240 ionization electrons per centimeter along a minimum ionizing track [12]. The drift velocity under our expected operating conditions should be $\approx 1 cm/\mu sec$ (figure 3). We anticipate from transverse diffusion, $\sigma_D \leq 45\mu m/cm^{\frac{1}{2}}$.

As currently envisioned, the RDC for the PEP-4 TPC will have 240 cells at the inner radius and 336 cells at the outer radius, corresponding to cell sizes of 1.50 *mm* and 2.90 *mm* respectively. Each cell will require two waveform sampling circuits, one for the anode and one for the pickup wire difference signal. The total channel count will be 1152.

2 Factors affecting spatial resolution

2.1 Mapping

In order to reconstruct charged particle trajectories from the information obtained on the wire triplets, it is necessary not only to be able to localize the centroid of the avalanche in the radial field region, but it is also necessary to understand how the linear field region is mapped onto the radial region. As a first approximation, we will assume a linear mapping of the coordinate x, parallel to the wire plane, and perpendicular to the wire axis, onto α, the azimuthal angle around the wire [13] (figure 2). To be precise, the mapping of x onto the azimuthal angle is not linear, nevertheless this approximation will be assumed to be valid for the present purposes.

The quantities one can measure are, as a function of time, the charge induced on the left and right pickup wires, L, and R, and on the anode wire, A. In order to turn these measurements into a determination of α, one needs either an accurate model or detailed measurements of how the induced charges will be distributed on the pickup wires. A detailed model of the charge induced on cathodes from an avalanche is possible, and has been attempted [14]. We will be content here, however, to present a naive approach which will form the basis for a parameterization of the pickup wire response. In this context we will use the asymmetry in the pickup wire response, normalized to the anode wire response, $\frac{L-R}{A}$, as a measure of the angle α.

When an electron cluster drifts into the high field region close to the anode, an avalanche will develop centered around the field line it follows in towards the anode. One of the advantages of some organic gases, such as DME, is the possibility that such avalanches are quite localized and thus can produce a sizable asymmetry. The ion cloud resulting from the avalanche will be centered around a particular angle, and will extend a few wire radii out from the anode. The pickup wires will both see a common signal which will be taken to be proportional to the length of the projection of the avalanche cloud onto the $\alpha = 0$ axis. Similarly, the difference in the pickup wire response, $L-R$, will be taken to be proportional to the projection of the cloud onto the $\alpha = \frac{\pi}{2}$ axis. Based on this argument, we can form a

parameterization of the normalized signal asymmetry in terms of α:

$$\frac{L-R}{A} = a \sin \alpha \tag{2}$$

If we assume a linear mapping of x onto α, one can then write

$$\frac{L-R}{A} = a_1 \sin a_2 x \tag{3}$$

where a_1 sets the relative normalization of the sense to the pickup wire response. For a given anode and field wire voltage, there will be some α_{max}, the maximum angle a field line from the linear region will have as it approaches the anode wire. This angle corresponds to x_{max}, the field line lying on the edge of the cell. This condition determines a_2:

$$a_2 = \frac{\alpha_{max}}{x_{max}} \tag{4}$$

For a fixed error in the ratio $\frac{L-R}{A} \equiv f$ one is interested in the corresponding error in coordinate determination. A constant error in f can result from both electronic noise and from limited avalanche statistics. In order to see how this propagates to errors in the spatial coordinate x, one can invert equation 3 to obtain:

$$x = \frac{1}{a_2} \sin^{-1} \frac{f}{a_1} \tag{5}$$

The error in x, δx, is given by:

$$\delta x \approx \frac{\partial x}{\partial f} \delta f \tag{6}$$

so,

$$\delta x \approx \frac{1}{a_1} \frac{x_{max}}{\alpha_{max}} \frac{\delta f}{\sqrt{1-(f/a_1)^2}} \tag{7}$$

From this one can qualitatively see that the resolution is approximately a constant if $(f/a_1)^2 \ll 1$. If, on the other hand, f/a_1 is close to 1, then the resolution has a non-trivial dependence on f; this can happen near the edge of the cell.

2.2 Diffusion, Electron Sharing

The transverse diffusion of electrons in the linear field region will degrade the resolution of the signal. In addition to this, as the swarm enters the radial drift region, because the field lines are getting closer together, the swarm will be heated, and will show a larger diffusion per unit drift length. Finally the contribution from the transverse spread of the avalanche must be taken into account. In dimethyl ether, the contribution of diffusion has been studied by Villa [4] in a linear field region. Figure 4 shows the results of his study. The minimum transverse diffusion expected in DME is $\approx 40\ \mu m/cm^{\frac{1}{2}}$.

Another factor affecting the spatial resolution of the chamber is electron sharing between adjacent cells (a *cell* being defined as the drift region mapped onto one sense wire). Electrons near the boundary of a cell can diffuse into neighboring cells, reducing the number of electrons collected, and thus reducing the pulse height measured. Due to a constant noise contribution, the position resolution will thus deteriorate. One possible way to circumvent this problem is to combine the signals from neighboring cells to regain some of the information lost in sharing. For tracks very near a cell boundary, the ratio of charge collected in neighboring cells is a sensitive measure of position and can be used as an alternative method.

A possible source of systematic error is local space charge caused by the avalanche process. This space charge can distort the electric field near the wire, changing the drift

path for electron clusters arriving later. This effect is likely to be significant only for tracks lying in a plane z = constant. Even a small polar angle causes the avalanche to run along the wire, spreading the ions along a distance large in comparison with the ion motion perpendicular to the wire.

3 Apparatus

In the first phase of studies, we wished to examine some of the fundamental aspects of operation of a chamber in dimethyl ether, and the feasibility of using pickup wires to localize avalanche coordinates. To this end we constructed a planar test chamber, and a point source of thermal electrons which could be positioned accurately at the edge of the drift volume. Figure 5 shows a schematic drawing of the wire plane and the electron source housing.

3.1 Wire plane

The drift geometry was defined by 2 copper cathode planes separated by 12 mm. A 2 in hole was machined onto the upper cathode plane to allow for motion of the electron source. The lower cathode plane was formed by copper plated onto a NEMA G-10 backing. A printed circuit board containing voltage distribution and blocking capacitors is sandwiched between two G-10 spacers. This circuit board held the wire plane.

The wire plane consisted of 34 wire triplets. No field shaping wires were used in this test chamber. The anode wires were 20 μm diameter gold coated tungsten. The pickup wires were 75 μm gold coated Cu-Be alloy. 1.5 mm separated the centers of adjacent wire triplets, and ± 250 μm separated the centers of the sense and pickup wires. Because of the spatial requirements on the printed circuit board, only 4 wire triplets could be instrumented. These triplets were located in the center of the wire plane, permitting uniform boundary conditions to be established in the regions where resolution tests were performed. The remaining 30 triplets had appropriate voltages distributed via buses on the circuit board.

The wire plane was pre-wound onto a pair of nickel flashed threaded brass bars which were separated by a meehanite (cast iron) spacing frame. During the winding, the wires were captured and held in place by the grooves in the bars. Anode wires were wound at 50 gm of tension and pickup wires were wound at 100 gm. The prewound wire frame then held the wires in position for the transfer to the circuit board. Epoxy beads held the wires onto the circuit board. After transfer to the circuit board, a test winding was inspected under a precision microscope and showed an RMS deviation of 2 μm from the theoretical wire locations.

When the chamber was in operation, the cathode planes were held at ground potential, and the sense and pickup wires were held at positive high voltage. The ratio of the sense to pickup voltages were determined by a single power supply hooked to a divider circuit. The ratio V_{pickup}/V_{sense} could be varied between 0.75 and 0.80. The potential corresponding to zero charge on the pickup wire results when V_{pickup}/V_{sense} was 0.79. Typically the pickup wires were run at $V_{pickup}/V_{sense} = 0.76$. At this ratio, the pickup wires become a source of field lines, leading to a more appropriate electric field. In a real sense, the pickup wires were providing the electric field lines that would be provided by the field wires if they had been present.

3.2 Electron source

To study the signals on the sense and pickup wires required a nearly pointlike source of thermal electrons which could inject these periodically into the drift region at reproducible locations. In addition, we wanted to measure the response as a function of the number of electrons arriving at the sense wire. To this end, a source of thermal electrons was designed and built, based on coronal discharges (Figure 6). The electron source consisted of a 75 μm

diameter Pt sphere at the end of a 50 μm Pt wire. The wire was connected to a high voltage source through 50 $G\Omega$ series resistor. The wire was held at negative high voltage, and was surrounded by a grounded brass sheath. On the end of the sheath closest to the wire plane was an electrode structure used to control the number of electrons passing into the drift volume. The other end of the sheath held a high voltage feedthrough and gas plumbing. The source contained an Ar-Isopropanol mixture at 1 atm. When the ball was held at a voltage of $\approx$ 1150 V, Geiger-like avalanches would occur periodically. Because of the long charging time ($RC \approx 0.1$ sec), it would discharge at a low frequency, approximately 10 Hz, acting as a relaxation oscillator. The isopropanol served to propagate the avalanche around the Pt ball, giving uniform response regardless of where the avalanche was initiated. The pulse observed on the wire with a fast preamp showed a rise time of 20 $nsec$.

The electrode structure was a pair of rectangular copper strips on a thin G-10 backing sandwiched between two thin brass disks. Small holes were placed in the center of the three disks to allow a passage for electrons to the drift volume. The hole closest to the Pt wire was 1/32 in in diameter. The copper steering electrodes flanked a 1/32 in hole in the G-10 disk. The hole closest to the wire plane was 15 μm in diameter in a .001 in thick brass disk. In a typical operating configuration, the brass disk bordering the drift region was held at 150 V. The electrode potentials could be separately varied between 7.2 and 78.6 V. An asymmetric potential setting for the steering electrodes moves the more intense core of the electron pulse away from the final aperture. In this manner, we could obtain yields of between 3 e^- and 300 e^- into the drift volume per discharge.

In order to reduce the effects of leakage of Ar-Isopropanol through the 15 μm hole, a flow of dimethyl ether was directed across the wire plane to remove any traces of unwanted gas. The entire source assembly was mounted onto a movable stage which could position it over the wire plane with $\approx$ 10 μm accuracy.

3.3 Electronics

Owing to spatial limitations, only one triplet of wires could be monitored at a time. Each wire in the triplet was instrumented with a blocking capacitor, a preamplifier, a variable gain shaping amplifier ($\tau = 800$ $nsec$), and a stretcher. The preamplifier had an integrating time of 20 μsec. Figure 7 shows a block diagram of the entire electronics chain.

The output of the wire channels served as inputs to an analog divider circuit which forms the ratio:

$$f \equiv \frac{L-R}{A} \tag{8}$$

where L,R, and A are voltage levels. The output, f , was also a voltage level. The divider circuit was based on a monolithic four quadrant multiplier (MC1594L), and exhibited a linear response for positive values of A ranging from 0.2 to 10. V, and for values of L and R in the range ± 10 V. Because the divider circuit had an intrinsically long response time ($\approx$ 20 μsec), it was necessary to stretch the output of the shaping amplifiers to 100 μsec to achieve a linear response. A delayed gate generator was used to clock the output voltage level, f into the pulse height analyzer, when the divider was in this linear range.

In general, two modes of operation were used. First, the raw output of each shaping amplifier could be connected to the input of the pulse height analyzer. In this mode, one could find the average pulse height as a function of the source location, to determine the individual response of each wire. The divider circuit was employed in the second mode of operation to obtain the quantity $\frac{L-R}{A}$ on a pulse by pulse basis. In either case, the spectrum of output pulse heights were sampled with a multichannel analyzer (LeCroy Model 3001).

The gain response of the wire channels were calibrated by coupling a square wave through a precision capacitor (4.43 pF) to the input of the preamplifiers. By pulsing all three channels at once, it was possible to measure the noise contribution of the signal processing chain for the ratio f.

4 Tests

Three basic measurements were performed. First the gain as a function of voltage was determined in DME using an Fe^{55} x-ray source (5.9 keV). Second, the responses of the sense and pickup wires were measured as a function of the electron source position, x. The ratio $\frac{L-R}{A}$ was taken on a pulse by pulse basis both for varied source locations and with a varied yield of electrons. During these tests, the chamber was run at 1 atm in dimethyl ether.

4.1 Gain calibration

An Iron-55 x-ray source (energy= 5.9 keV) was used to calibrate the gain. We have assumed that the x-ray conversion yields 200 ionization electrons in our calibration. Figure 8 shows the pulse height spectrum seen on the sense wire when running at a voltage of 3500 V. From the electronics gain calibration, we could calculate the effective number of electrons at the input of the preamplifier (integration time = 20 μsec). At different voltages we could then estimate the electron yield at the wire and thus infer the gain. The average pulse height response as a function of sense wire voltage is plotted in figure 9. With the present set-up, sense wire signals begin to appear above electronic noise at $\approx$ 3200 V. Gains were measured with voltages as high as 5200 V. As one can see from figure 9, the curve begins to depart from exponential behavior above 4500 V. This is most likely due to space charge limitations.

By knowing the gain as a function of voltage, from the calibration we can then estimate (to an accuracy of $\approx$ 20 %) the yield from the thermal electron source.

4.2 Mapping

Using the electron source in a mode in which 200 electrons were ejected per discharge, detailed maps of wire response as a function of source position, x, were taken for the anode and both pickup wires. These data were taken at a gas gain of 10^3. The anode wire map (mean pulse height as a function of electron source position) is shown in figure 10. The most prominent feature of this map is the drop in the collected wire signal near the edge of the cell. This is due to electron sharing with the neighboring cells. The width of this region is consistent with the expected diffusion in DME (sharing region $\approx 100\mu m$ wide). One can also see from this map that the gain is larger on the edges of the cell than in the center. This is a result of a slightly higher density of field lines as $\alpha \rightarrow \frac{\pi}{2}$, induced by the charge on the pickup wires. The left and right pickup wires were wound from different batches of wire, with a small difference in the diameters of the two batches. This gives rise to a small asymmetry in the sense wire response, visible in figure 10. The pickup wires also show the same asymmetry, giving a cancellation in taking the ratio $\frac{L-R}{A}$.

In figure 11, we have plotted the mean pulse height seen on the pickup wires as a function of the position of the electron source. One can clearly see the asymmetry in the response of the pickup wires, and the region dominated by the sharing of electrons with neighboring cells. Qualitatively, the response exhibits the expected behavior, namely that there is some common component of the signal seen on both wires, and some asymmetry in the response.

By taking the ratio $\frac{L-R}{A}$ for the mean pulse heights found on the sense and pickup wires as a function of x, it is possible to construct the asymmetry map described earlier. Figure 12 shows this asymmetry, and the result of a fit to the function:

$$\frac{L-R}{A} = a_1 \sin a_2(x - a_3) \tag{9}$$

The constant a_3 was used to determine the center of the cell, the other constants, a_1, and a_2 describe the overall normalization and the mapping of x onto α. The best fit of this function to the data gives:

$a_1 = 0.848 \pm 0.04$

$a_2 = 1.66 \pm 0.1$

$a_3 = 10.06 \pm 0.01$

$\chi^2 = 31$ (21 degrees of freedom)

The results of the fit agree quite well with the naive model described above. The value of the constant a_1 implies a maximum asymmetry of about 80 % for these operating conditions and geometry. The value of the constant a_2 implies that for $x_{max} = 750\ mm$, $\alpha_{max} = 71 \pm 4^o$.

4.3 Pulse by pulse mapping

With the divider circuit, we measured the asymmetry , $\frac{L-R}{A}$, on a pulse by pulse basis for different locations of the electron source. From these mappings, it is also possible to make asymmetry plots of f as a function of x. One such plot is shown in figure 13, along with a best fit to the asymmetry function 9 described above. In this case, the vertical axis is now the peak channel number on the pulse height analyzer. Because the channel number corresponding to $L = R$ is not known *a priori* , an extra parameter, a_4, is needed to fit the $f = 0$ point of the asymmetry to the corresponding PHA channel number. The parameters of the fit are:

$a_1 = 109.9 \pm 0.7$

$a_2 = 1.57 \pm 0.01$

$a_3 = 13.53 \pm 0.02$

$a_4 = 125 \pm 3$

$\chi^2 = 17.7$(19 degrees of freedom)

A comparison with the previous fit, based on average pulse heights , shows good agreement. By evaluating the residuals to the fit of the sinusoid we find an RMS deviation of $\approx 5\ \mu m$ from the best fit curve. This demonstrates that even with a simple model of the field line mapping that one can understand quite well the asymmetry response, and use this information to reconstruct the location of the original electron cluster.

4.4 Resolution vs. number of electrons

In the next stage of tests we varied the number of electrons per discharge, and made pulse by pulse measurements of the asymmetry. All scans were performed with the electron source located at 300 μm intervals. In the linear range of f, the distance scale could be determined from the peak separations. From this information, we could extract the resolution in microns by measuring the widths of the distributions. Figure 14 shows three such scans for varying numbers of electrons injected into the drift volume. From the figure, it is clear that the resolution is degraded as the number of electrons in the swarm decreases.

The noise limit of the resolution was found from pulsing the inputs of the sense and pickup wires. This contribution was $\approx 30\ \mu m$ (FWHM). The results of these measurements are shown in figure 15, by plotting the width of the peaks (FWHM) as a function of $1/\sqrt{n_e}$. The intercept for an infinite number of electrons is consistent with our noise measurements. Extrapolation to an avalanche equivalent to one parent electron yields a FWHM of $260 \pm 10\ \mu m$. The data with small numbers of electrons were taken with a rather high E/p, about 8, corresponding to a drift interval diffusion contribution of $\approx 65\ \mu m$ RMS. Subtracting in quadrature gives a value of $88 \pm 10\ \mu m$ RMS for the equivalent spatial resolution contribution

for a single electron avalanche under these conditions. Expressed in angular coordinates at the anode wire, the equivalent angular resolution for a single electron avalanche corresponds to 8 ± 1^{o} RMS.

5 Discussion

These tests demonstrate that the asymmetry in the response of the pickup wires can be used to determine avalanche coordinates with good precision. From the information obtained above we now have a measurement of the combined contributions of electronic noise, diffusion and avalanche growth to the spatial resolution from a single swarm of electrons. We are now in a position to estimate the potential tracking resolution of the radial drift chamber. In 1.5 atm of DME, we expect $\approx$ 180 e^{-} per centimeter of track length. These electrons will drift at a velocity of approximately 1 $cm/\mu sec$, corresponding to an E/p of 4 $V/cm - Torr$, near the minimum in transverse diffusion. Assuming a sampling rate of 33 MHz, this gives a yield of 6 e^{-} per sample. From figure 15, we estimate an accuracy of 40 μm (RMS) per sample. If systematic effects are assumed negligible, with 30 samples (1.0 cm of path), we derive a tracking accuracy of 8 μm. Clearly, there may be a large gap between this calculation and what can be realized in an actual detector, but this does indicate the potential resolution of a chamber which uses the information from every electron along the length of a charged particle track. Because the resolution of this technique should follow a $(\text{pressure})^{-\frac{1}{2}}$ dependence for both the diffusion and statistical contributions, the resultant $(\text{pressure})^{-1}$ dependence offers the prospect of resolution values in the few micron range at modest overpressures.

In addition to the application discussed here, this technique may be valuable for other low crossing-rate colliding beam experiments.

We gratefully acknowledge the assistance of Ed Lampo, Armi Meuti and Garth Smith in building the apparatus. This work was supported by the U.S. Department of Energy under Contracts No. DE-AC03-76SF00098 and DE-AC02-76ER0330-Task B.

Bibliography

[1] G. Charpak, D. Rahm, H. Steiner, Nuclear Instrum. Methods, **80** , 13 (1970).

[2] J. Fischer, H. Okuno, and A. H. Walenta, IEEE Trans. Nucl. Sci., **NS-25** , 794 (1978).

[3] J. Marx and D. Nygren, Physics Today, **31** 10 (1978).

[4] F. Villa, Nuclear Instrum. and Methods, **217** , 273 (1983); M. Basile, *et al* , CERN-EP/85-40 (1985).

[5] D. R. Nygren, TPC note TPC-LBL-84-12 (1984).

[6] H. Okuno, J. Fischer, V. Radeka, A. H. Walenta, IEEE Trans. Nucl. Sci., **NS-26** , 160 (1979).

[7] J. Sanada, Nuclear Instrum. and Methods, **196** , 23 (1982).

[8] M. Matoba, T. Hirose, T. Sakae, H. Kametani, H. Ijiri, T. Shintake, IEEE Trans. Nucl. Sci., **NS-32** , 541 (1984).

[9] T.L. Cottrell, and I.C. Walker, Trans. Faraday Soc., **61** , 1585 (1965).

[10] A. H. Walenta, talk given at the 1981 ISABELLE Summer Workshop at Brookhaven National Laboratory; A. H. Walenta, Proceedings of the International Conference on Instrumentation for Colliding Beam Physics, SLAC Report 250, 34 (1982).

[11] J. Va'vra, CERN EF/84-17 (1984).

[12] J. Fehlman, and G. Viertel, 'A compilation of data for drift chamber operation,' ETH, Zurich (1984).

[13] G. A. Erskine, Nuclear Instrum. and Methods **105** , 565 (1972).

[14] J. S. Gordon and E. Mathieson, Nuclear Instrum. and Methods, **227** , 267 (1984).

Figure Captions

Figure 1: Cross section of the radial drift chamber. A central cathode divides the chamber into two drift regions. Inside the cathode, tracks drift to a set of wires at the inner radius. Outside the cathode, tracks drift out to a set of wires on the outer radius. The innermost shell is formed by a beryllium beam pipe.

Figure 2: View of one cell and associated wire triplet, consisting of a pair of pickup wires and one sense wire. Field wires at the cell boundaries are employed to reduce cell-to-cell cross talk, enchance gain, and optimize the electric field configuration. As shown, the pickup wires are at a neutral potential. A cluster of electrons from a charged particle will drift to the anode wire and form an avalanche centered around some azimuthal angle, α. The maximum angle, α_{max}, corresponding to field lines originating near the cell boundary, is determined by the relative potential on the anode and field wires.

Figure 3: Drift velocity of ionization electrons in dimethyl ether as a function of E/p from reference [4].

Figure 4: Results of a study of transverse diffusion of electrons in DME, taken from reference [4].

Figure 5: Test apparatus used to investigate the localization of avalanche coordinates. A source of thermal electrons mounted on a movable stage could deposit an electron swarm at different positions over a plane of wire triplets.

Figure 6: Schematic view of the thermal electron source. The source consisted of a 50 μm diameter ball at the end of a 20 μm wire, and was operated in an atmosphere of Ar-Isopropanol. The ball was connected to a high voltage power supply through a 50 $G\Omega$ series resistor. The system would act as a relaxation oscillator, with coronal discharges from the ball occuring at at rate of $\approx$ 10 Hz. Some electrons from the discharge pass steering electrodes and through a 15 μm aperature into the drift volume. Depending on the potentials on the steering electrodes, the source could produce a yield of between 3 and 300 electrons per discharge.

Figure 7: Block diagram of electronics used in testing spatial resolution. A parallel chain consisting of a blocking capacitor, a preamplifier, a shaping amplifier, and a stretcher were used to measure pulses on the wires. An analog divider circuit was used to determine the asymmetry in the pickup wire response on a pulse by pulse basis. The output of the divider circuit was read into a pulse height analyzer.

Figure 8: Iron-55 pulse height spectrum measured in DME. The wires were operated at 3500 V.

Figure 9: Effective number of electrons seen at the anode wire as a function of operating voltage for Fe^{55} x-rays in DME. Note the departure from exponential behavior above 4500 V.

Figure 10: Plot of pulse height seen on the anode wire, A, as a function of the location, x, of the electron source. The loss of signal near the edge of the cell is due to sharing of electrons with neighboring cells through diffusion . The small asymmetry in the left-right response of the sense wire is due to different batches of wire used in winding the left and right pickup wires.

Figure 11: Map of the pickup wire response, L and R, as a function of the position of the electron source. One can clearly see the asymmetry due to the angle of the avalanche around the wire.

Figure 12: Values of $(L-R)/A$ taken from averaged pulse heights on pickup and sense wires as a function of electron source location. Also shown is the result of a fit to a sinusoid.

Figure 13: Asymmetry map found using the analog divider circuit. The curve superimposed is the result of a best fit to a sinusoid (see text for parameterization).

Figure 14: Results of several scans of the electron source (300 μm intervals) with varying numbers of electrons per discharge. Each peak in the figure corresponds to values of $(L-R)/A$ taken with the gun in one location. The top scan is with 200 electrons, the middle is with 50 electrons, and the lower scan is with 8 electrons per discharge. The loss of resolution with fewer electrons is evident.

Figure 15: Resolution as a function of $\frac{1}{\sqrt{n_e}}$. The intercept of the curve at $n_e = \infty$ is consistent with the noise contribution to our position resolution.

Figure 1

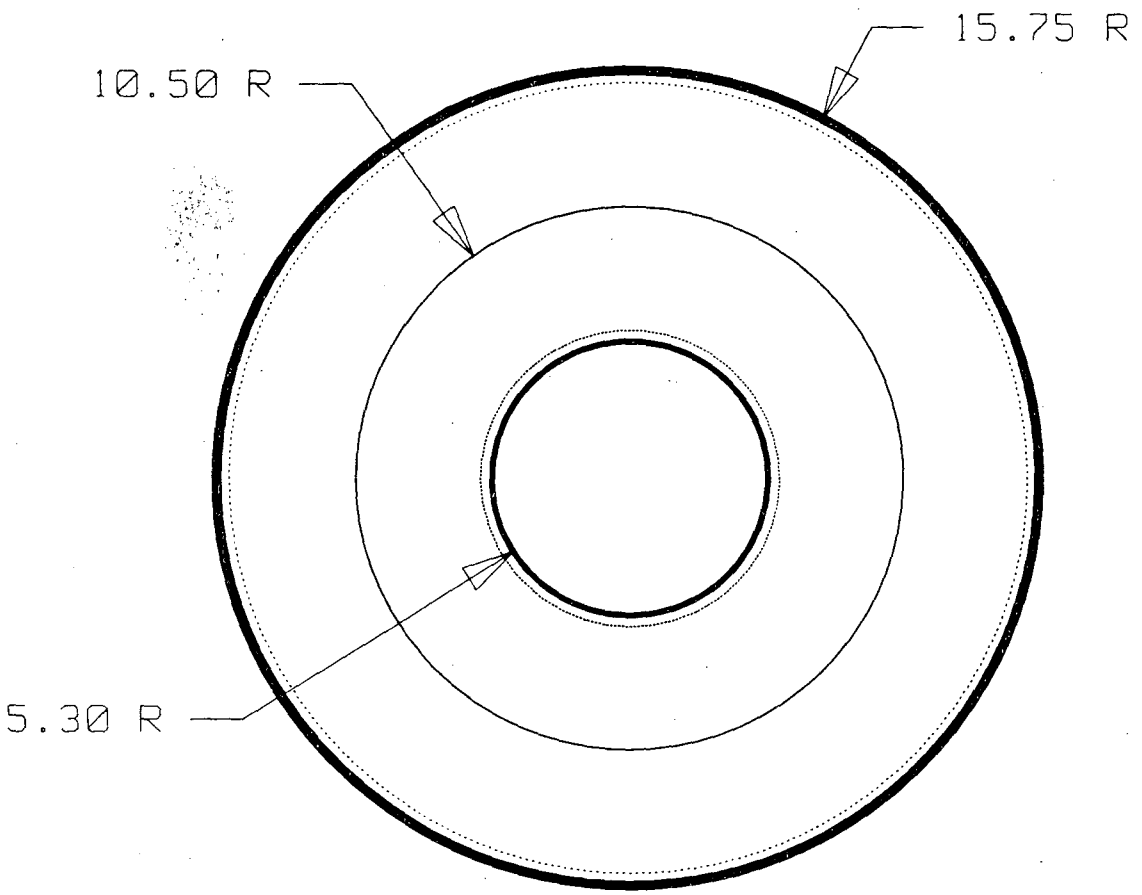

XBL 853-1905

Figure 2

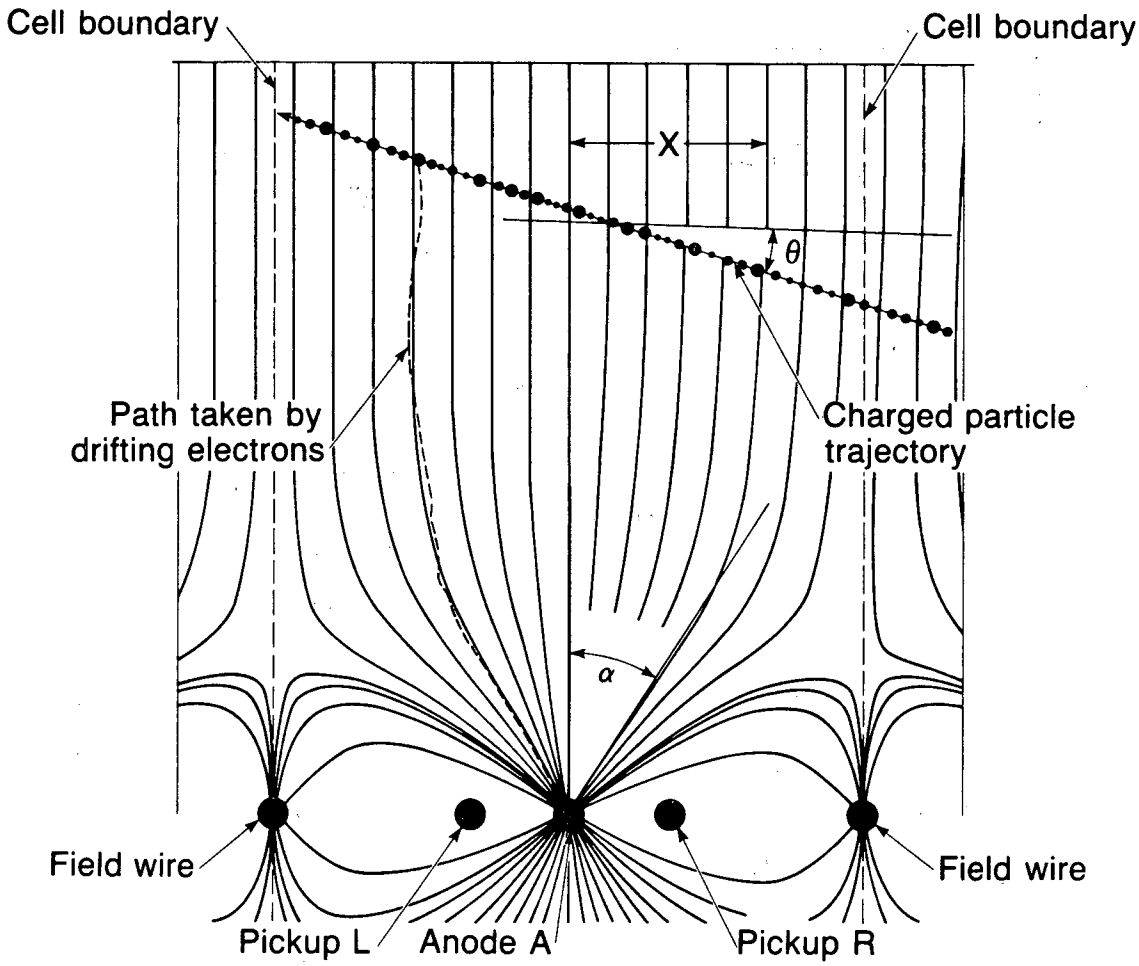

XBL 854-11065

Figure 3

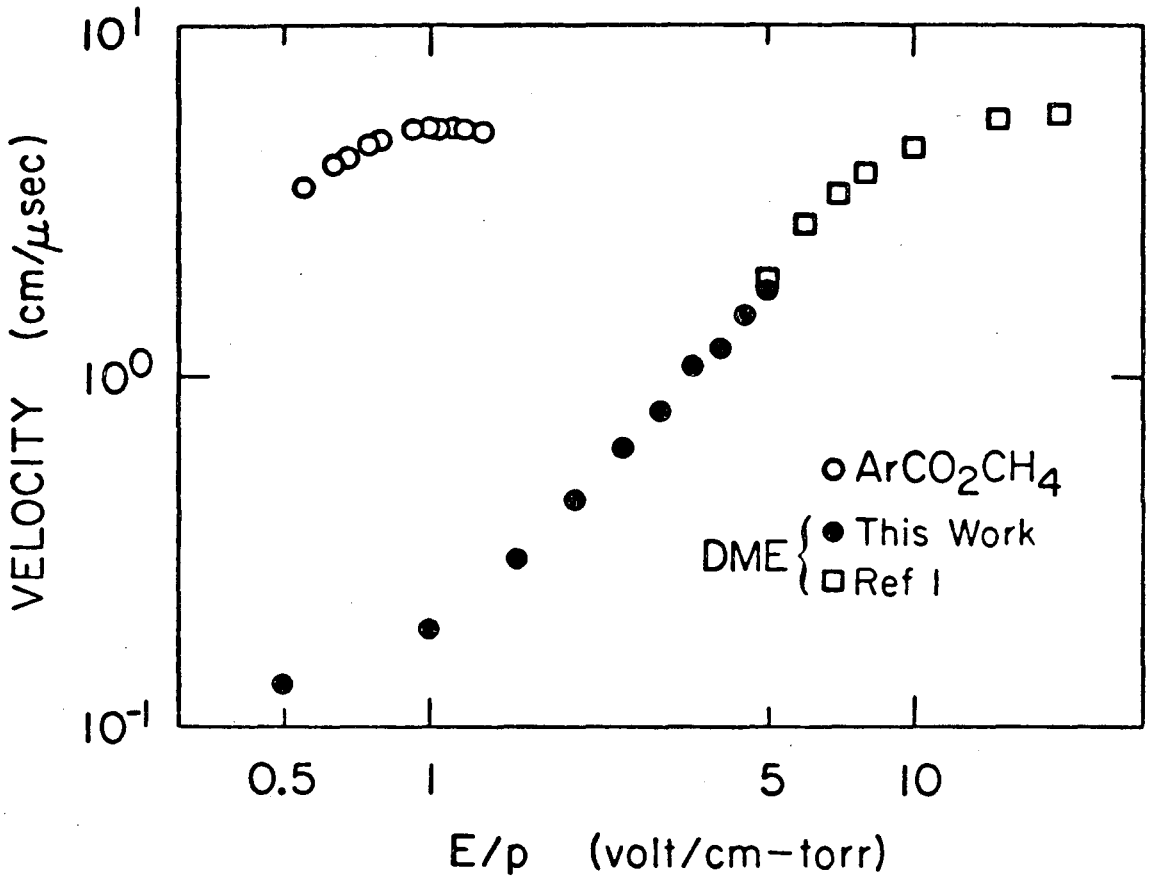

XBL 854-2114

Figure 4

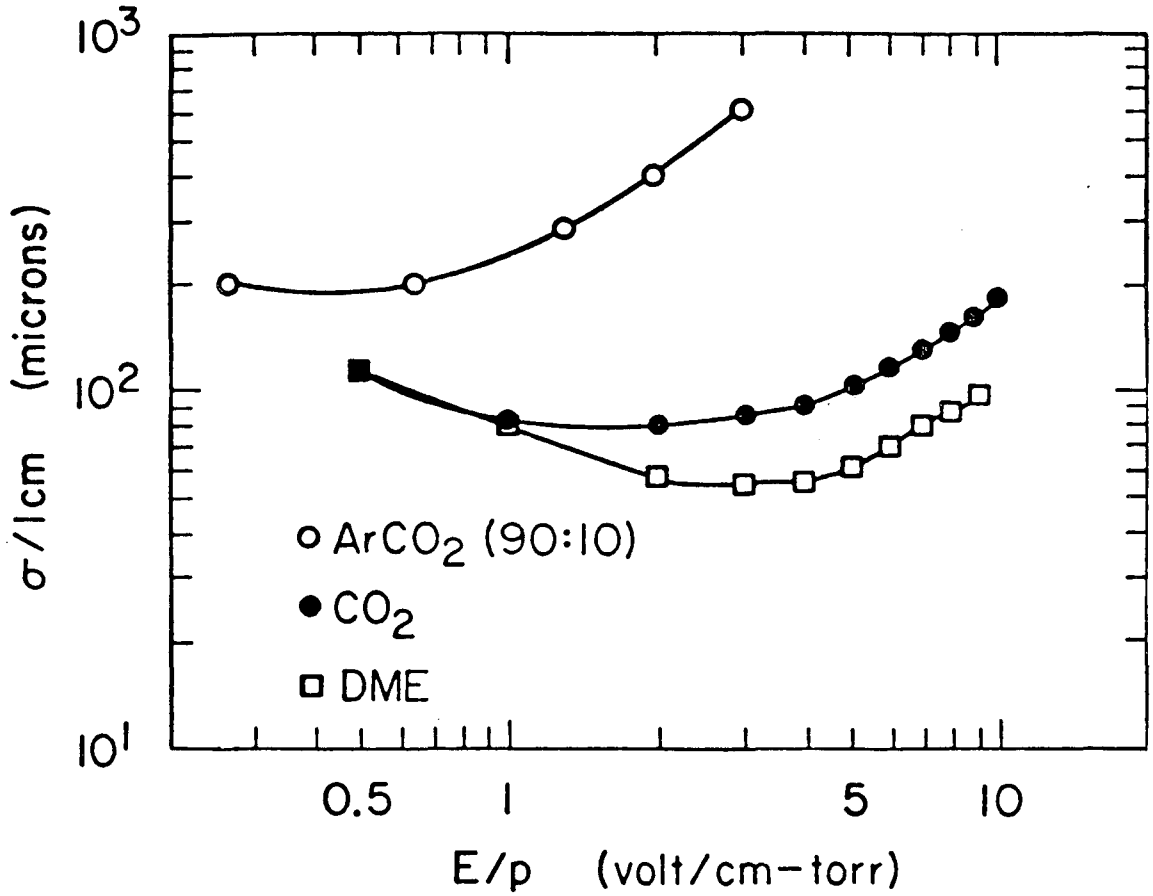

XBL 854-2113

Figure 5

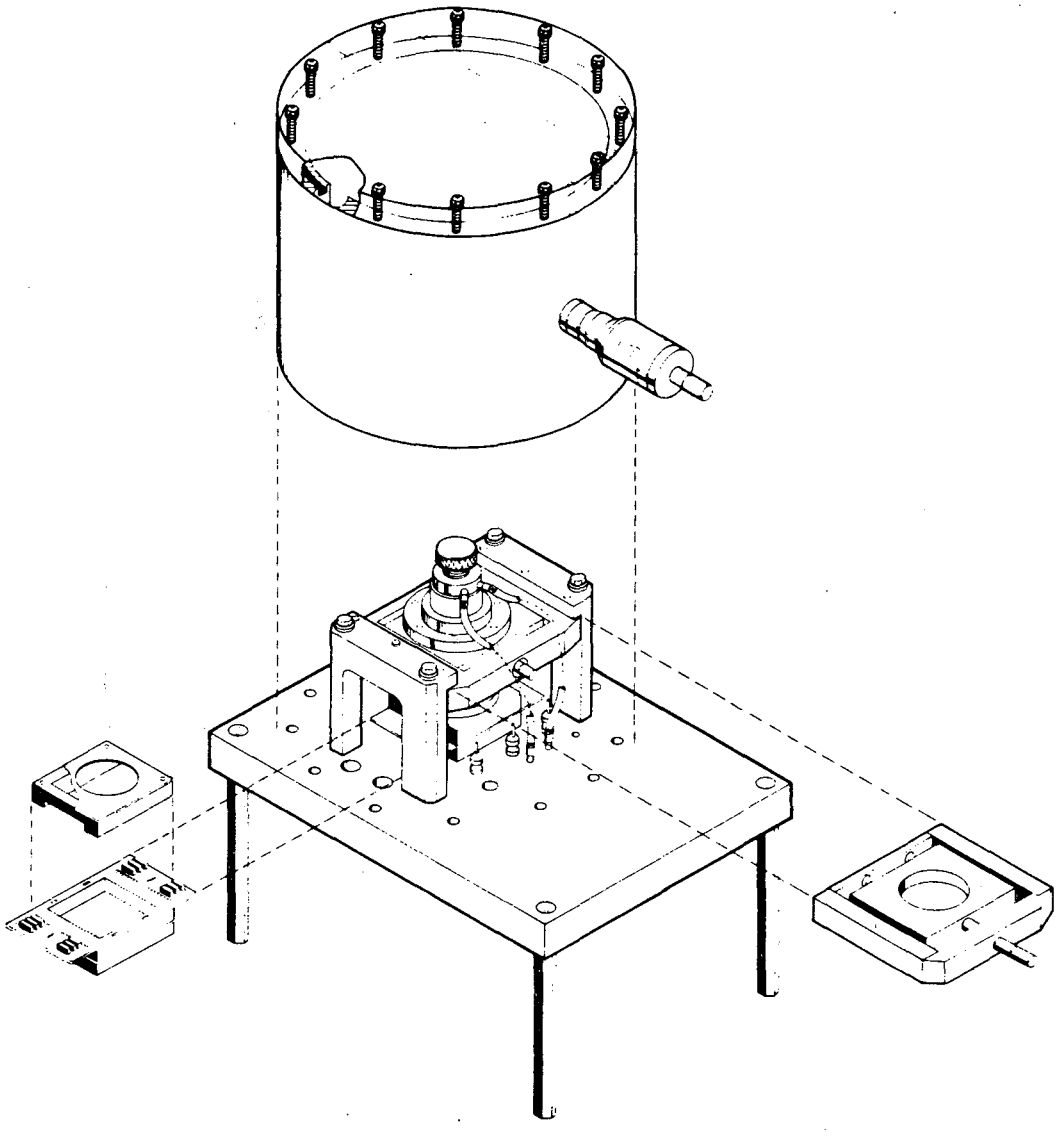

XBL 853-1904A

Figure 6

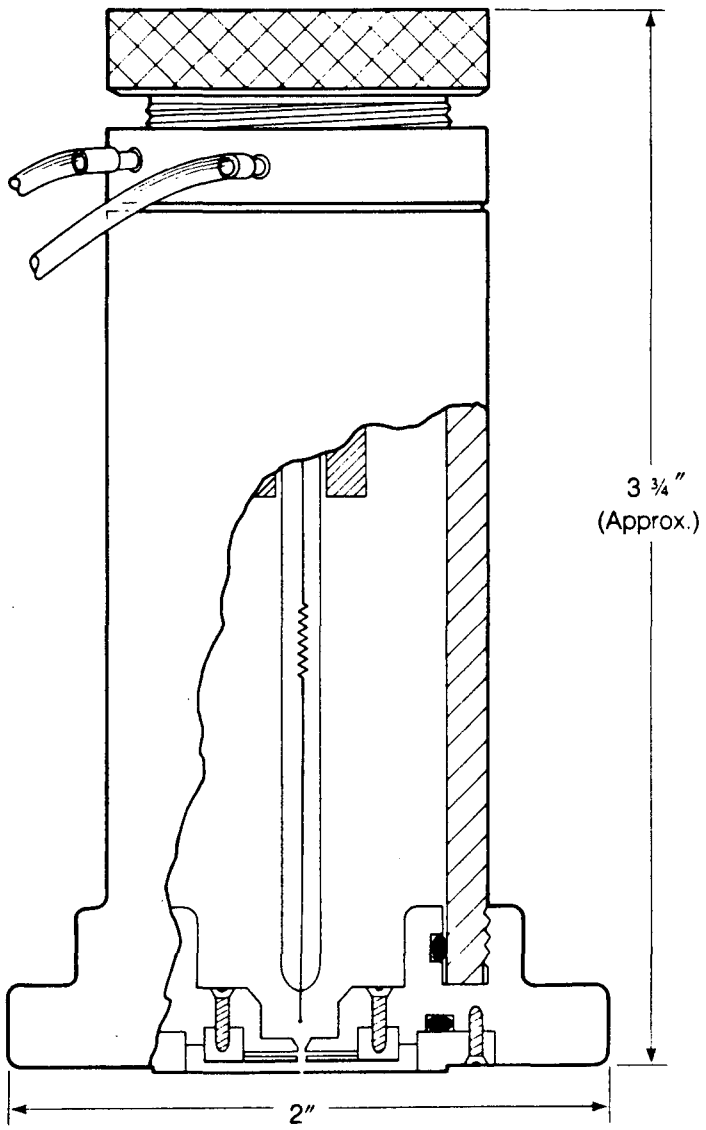

SMALL APERTURE VARIABLE YIELD
THERMAL ELECTRON SOURCE

Figure 7

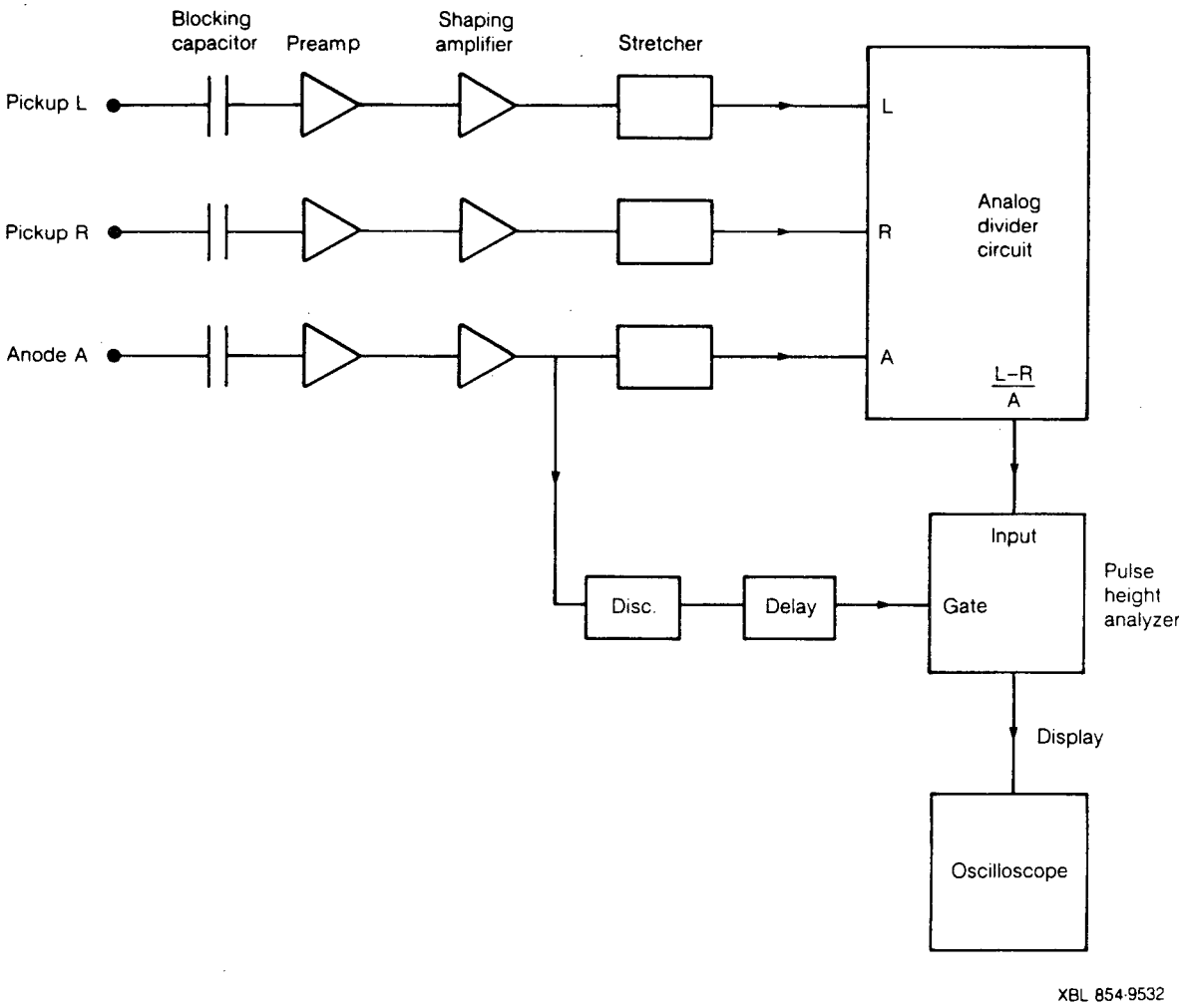

XBL 854-9532

Figure 8

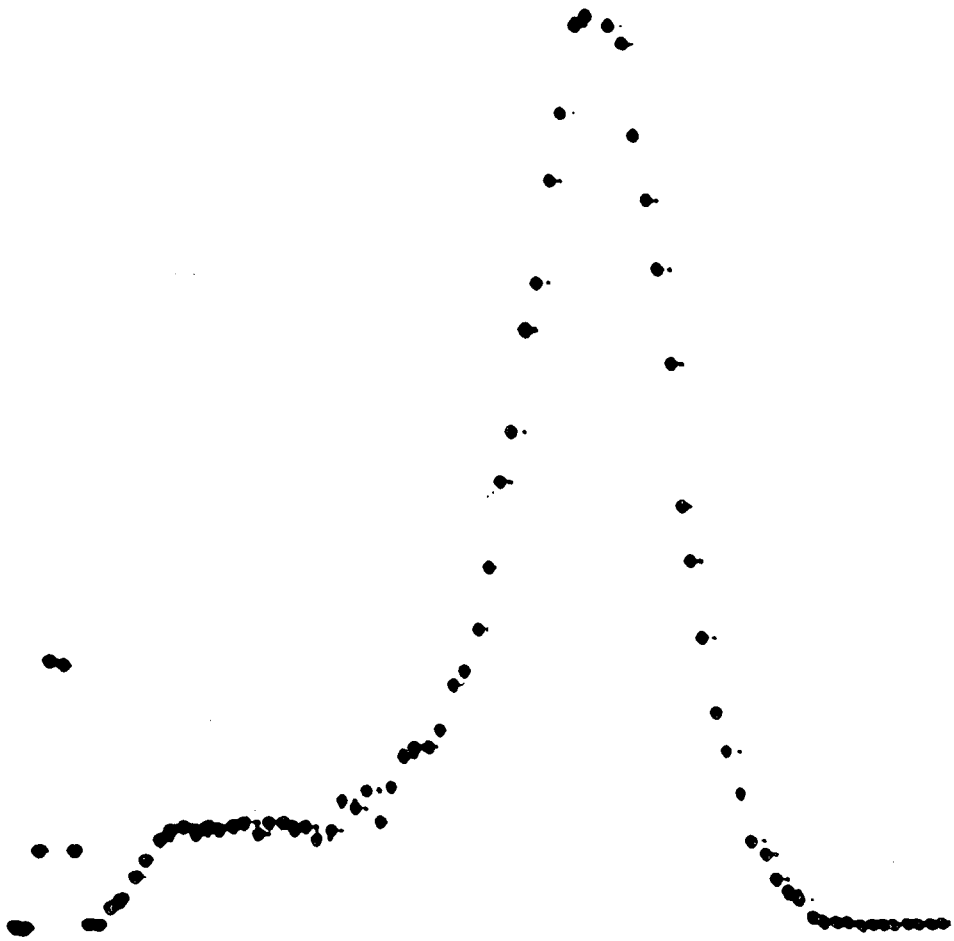

Figure 9

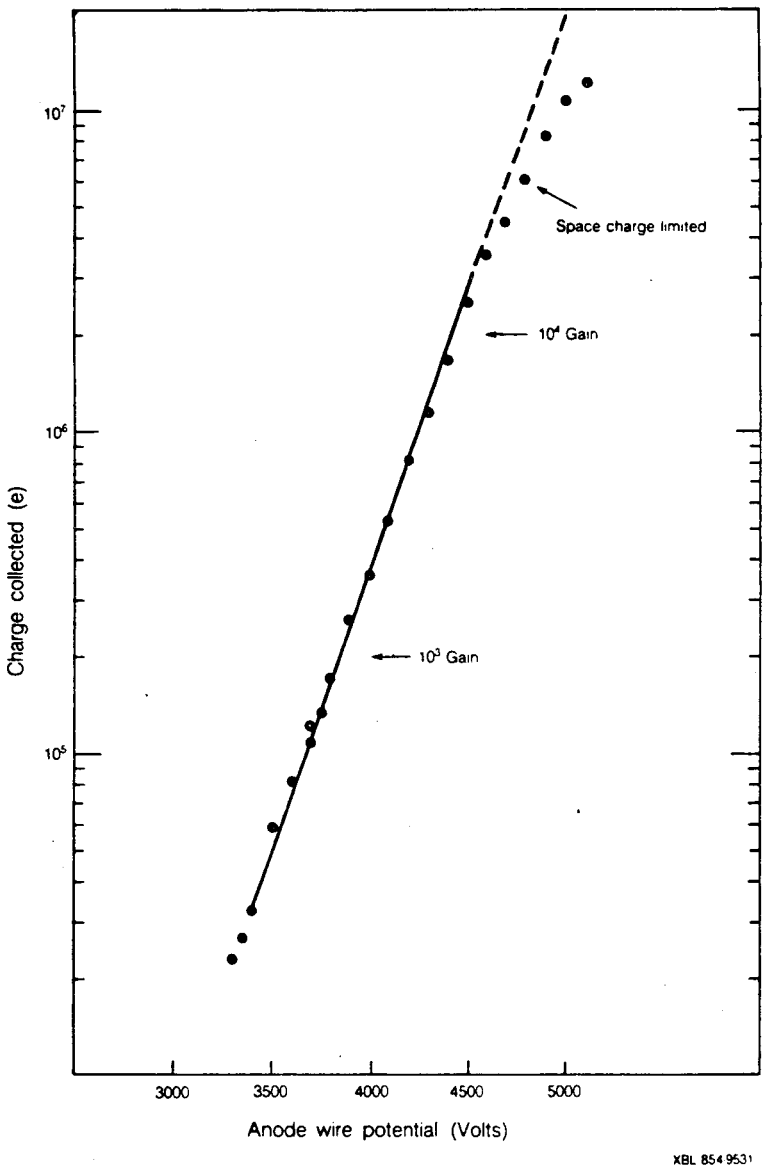
Charge collected (e)
10^7
10^6
10^5
Space charge limited
10^4 Gain
10^3 Gain
3000
3500
4000
4500
5000
Anode wire potential (Volts)
XBL 854 9531

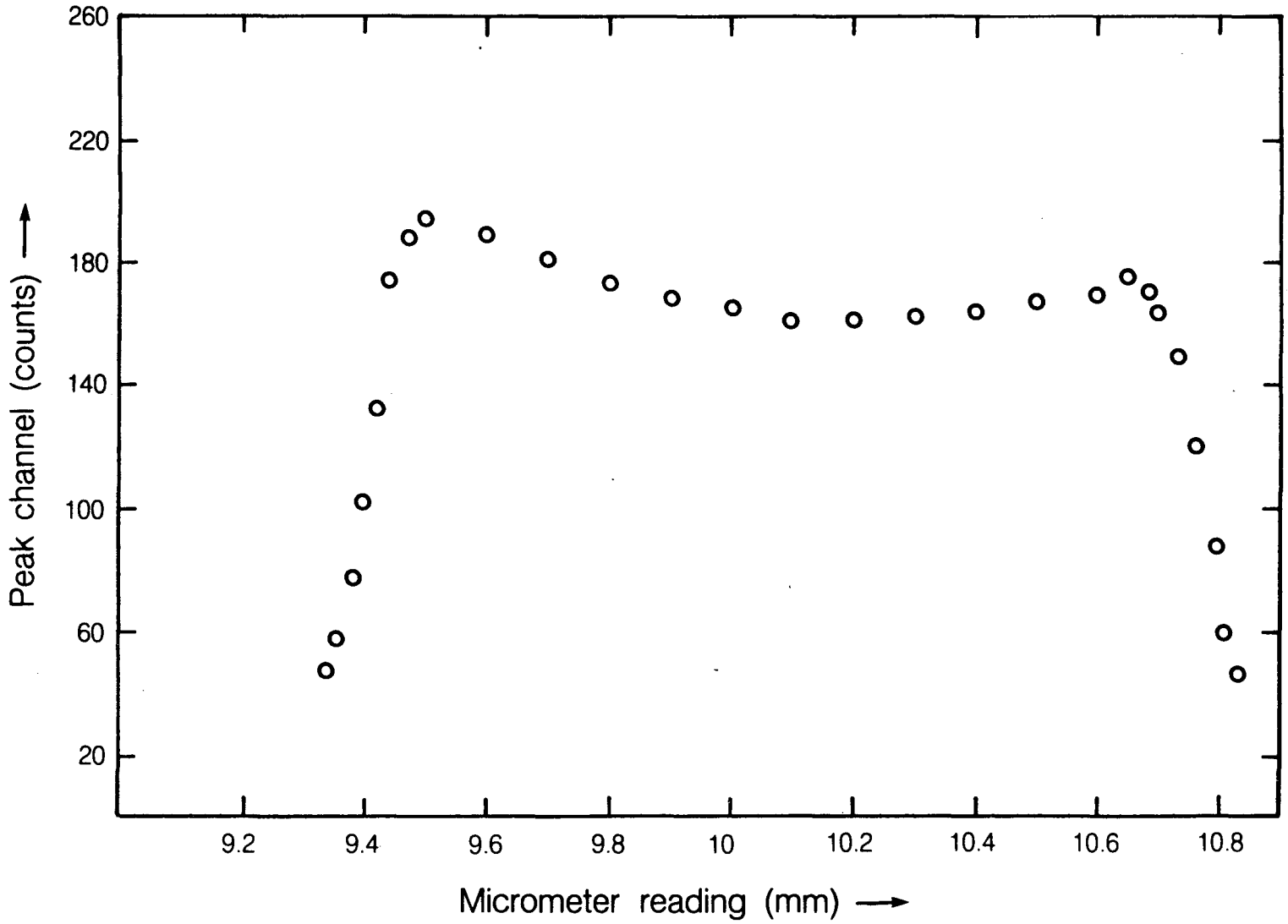

XBL 854-9530

Figure 10

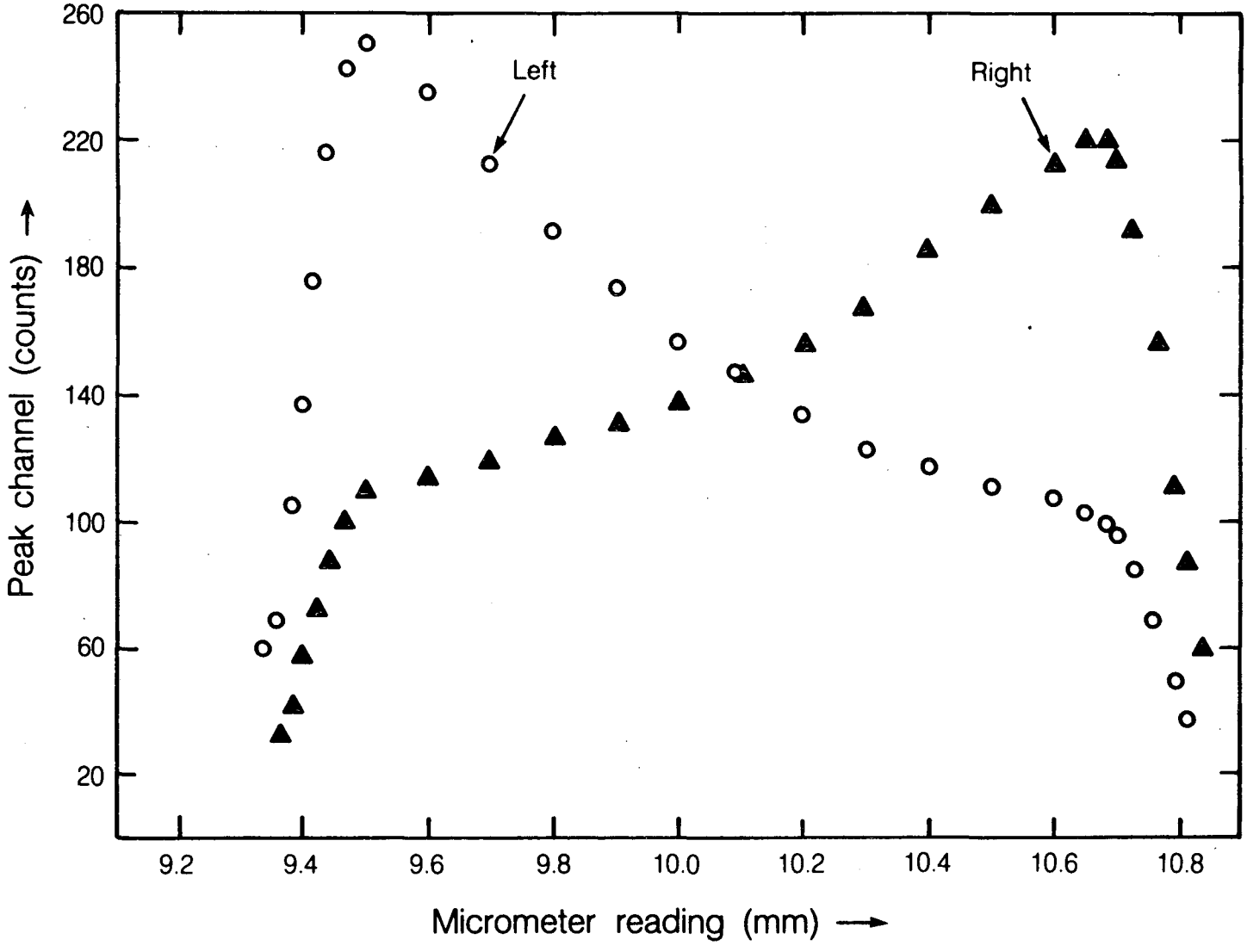
260
220
180
140
100
60
20
Peak channel (counts) →
Left
Right
9.2
9.4
9.6
9.8
10.0
10.2
10.4
10.6
10.8
Micrometer reading (mm) →
XBL 854-9529

Figure 11

Figure 12

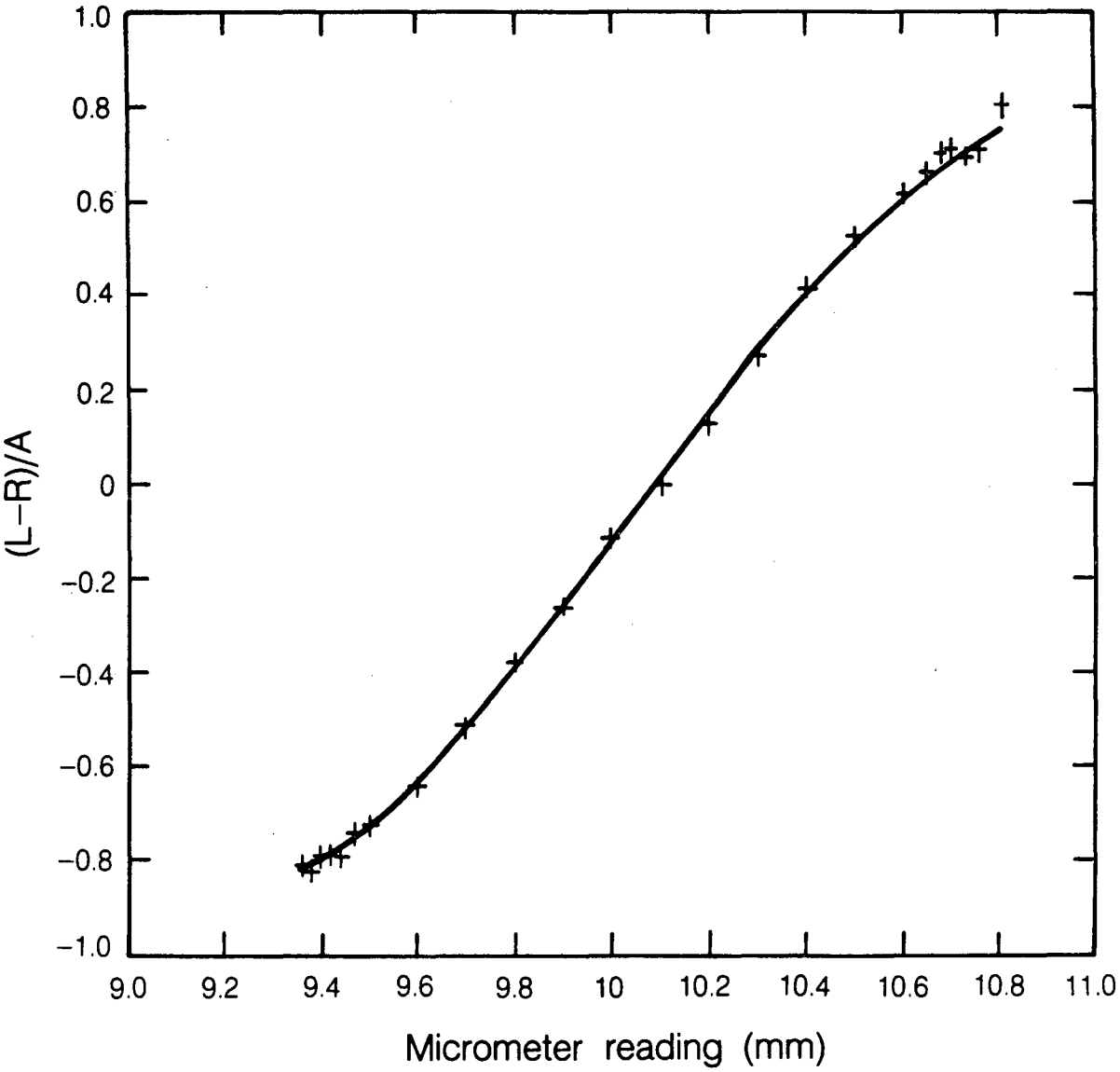

XBL 854-9528

Figure 13

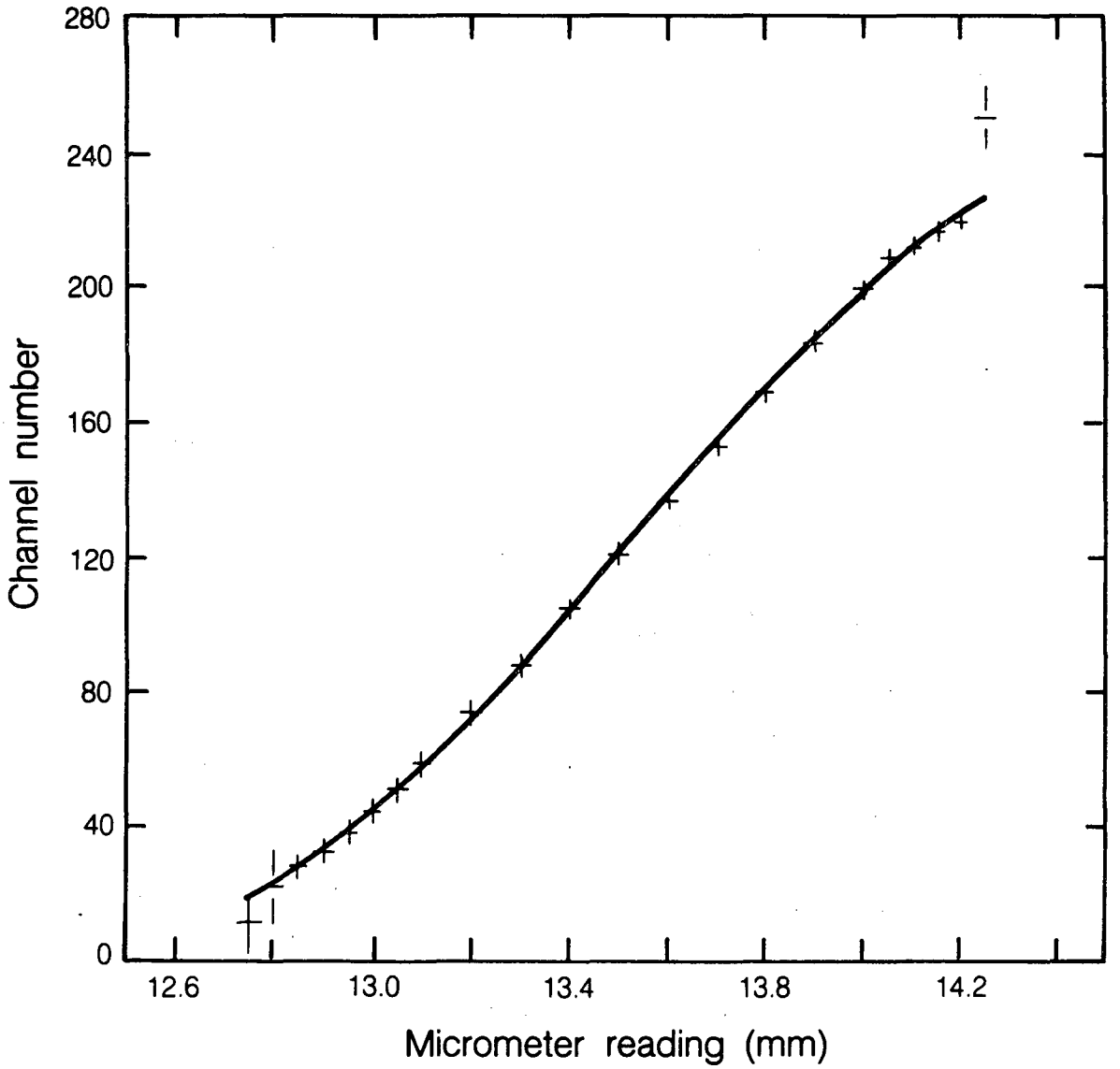

XBL 854-9527

Figure 14

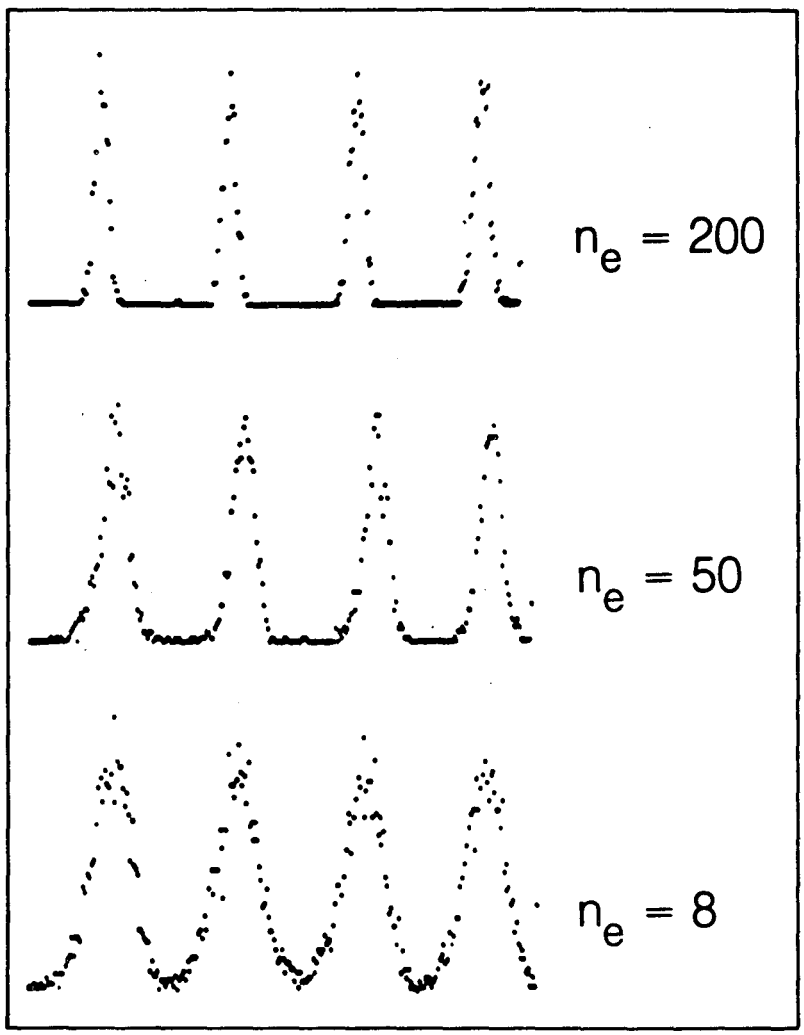

XBL 854-8853

Figure 15

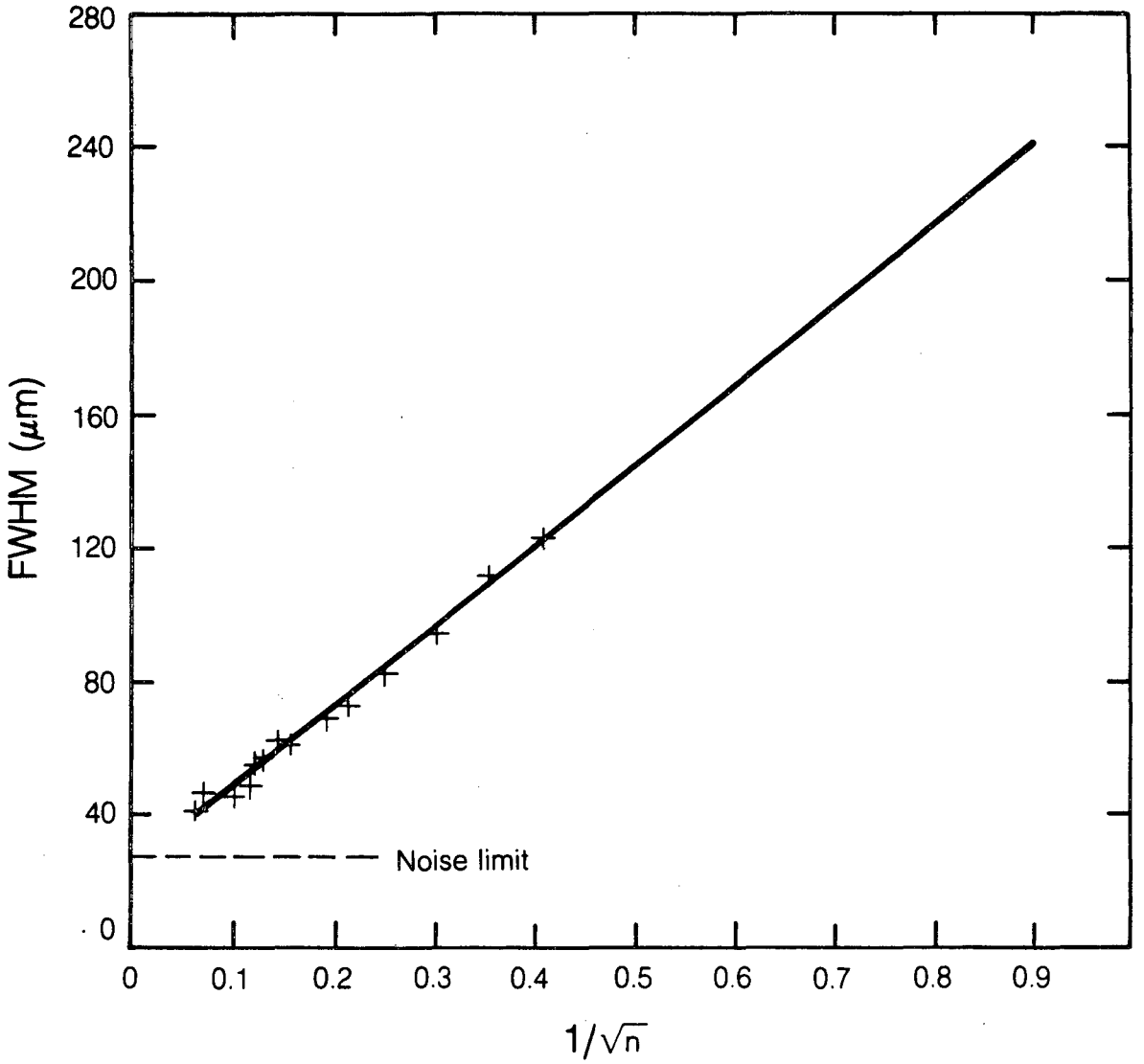

XBL 854-9526

LAWRENCE BERKELEY LABORATORY
TECHNICAL INFORMATION DEPARTMENT
UNIVERSITY OF CALIFORNIA
BERKELEY, CALIFORNIA 94720